Thermosensitive Molecular, Colloidal, and Bulk Interactions Using a Simple Surfactant

*Thomas E. Kodger, and Joris Sprakel**

Efficient use of (nano)particle self-assembly for creating nanostructured materials requires sensitive control over the interactions between building blocks. Here, a very simple method for rendering the interactions between almost any hydrophobic nano- and microparticles thermoswitchable is described and this attraction is characterized using colloid probe atomic force microscopy (CP-AFM). In a single-step synthesis, a thermoresponsive surfactant is prepared that through physical adsorption generates a thermosensitive brush on hydrophobic surfaces. These surface layers can reversibly trigger gelation and crystallization of nano- and microparticles, and at the same time can be used to destabilize emulsions on demand. The method requires no chemical surface modification yet is universal, reproducible, and fully reversible.

1. Introduction

Nanoparticles form versatile building blocks for the creation of structured materials; for example, ordered arrays of colloidal and/or nanoparticles display a distinct photonic bandgap, forming photonic crystals.[1] Similarly, the shimmering colors found in nature in a variety of beetles and butterflies are created through locally ordered assemblies that give rise to their vivid physical color.[2] Even fully disordered packings of nanoparticles display fascinating properties, from the trapping of light, so-called Anderson localization,[3] to related phenomena such as random lasing.[4] The use of nanoparticles for these applications is appealing as these structures may be formed spontaneously through self-assembly, without the requirement for cost- and labor-intensive lithographic methods.[5]

Assembly of nanoparticles into ordered, or disordered, packings can be achieved in a variety of ways. Some of these require external energy input, such as methods involving capillary shaping of crystals at the drying front of a fluid meniscus[1] or methods that use external fields to drive ordering, such as electric fields[6] or shear and compressional flow.[7] Alternatively, the formation of nano- and microstructured materials may be achieved by tuning or triggering the attractive and/or repulsive interactions between the nanoparticles in the absence of any external driving forces, an approach known as self-assembly. Tunable forces between the surfaces of nanoparticles greatly enhance the fidelity of the self-assembly process. In recent years, inspiration has been taken from nature, using complementary DNA strands to trigger the attraction-driven self-assembly of DNA-coated particles. While successful and versatile, the high binding affinity of the complementary DNA strands inhibits crystallization and crystal formation occurs only in a very small window of environmental parameters.[8] Moreover, protocols for grafting biomolecules to the surface of nanoparticles typically involve several chemical modification steps.[9] Also synthetic polymers present at a particle surface may be used to induce self-assembly. One well-described approach is the grafting of polymer chains from the surface, e.g., using atom-transfer radical polymerization.[10] For these methods, several chemical modifications are required to achieve surface-anchored initiators and grafted chains. These examples illustrate a need for straightforward and inexpensive methods with which the interactions between arbitrary colloidal particles can be made precisely responsive to environmental triggers.

The availability of such methods would not only have important applications in the fields of nanostructured colloidal materials but also in industrial applications. Many consumer products, such as coatings,[11] foods,[12] and cosmetics, use networks of weakly aggregated particles, known as colloidal gels, to impart a soft-solid mechanical behavior to these otherwise fluid products. If the attraction forces between the particles, ultimately responsible for the network formation of the particles, were tunable, it would greatly improve not only processability but also the control of the material properties.[13] In the same fashion, enviromentally triggerable attractive forces between microscopic particles could be used to trigger on-demand phase inversion of emulsions,[14] which may greatly facilitate emulsion-based separation processes, film formation in drying emulsion paints, and the recovery of crude oil from waterflooding-based enhanced oil recovery.[15] In this paper we demonstrate a novel and facile method for rendering the interactions between almost any type of nanoparticles, ranging from polymeric latex particles to emulsion droplets, thermoresponsive. This is accomplished by the one-pot synthesis of a thermoresponsive surfactant, through chain-transfer polymerization of poly(*N*-isopropylacrylamide), which is subsequently spontaneously adsorbed to the surface of nanoparticles. The spontaneously assembled thermoresponsive

T. E. Kodger
School of Engineering and Applied Science
Harvard University
9 Oxford Street, Cambridge MA, 02138, USA
Prof. J. Sprakel
Laboratory of Physical Chemistry and Colloid Science
Wageningen University
Dreijenplein 6, 6703 HB Wageningen, The Netherlands
E-mail: joris.sprakel@wur.nl

DOI: 10.1002/adfm.201201515

brush instantaneously imparts a temperature-tunable attractive potential between particles. We directly quantify these interactions using colloidal probe atomic force microscopy (CP-AFM). To demonstrate the versatility of our method, we show that it reversibly triggers gelation and crystallization in nanoparticle dispersions and induces phase inversion on-demand in an otherwise stable oil-in-water emulsion.

2. Results and Discussion

We use the well-known lower critical solution temperature (LCST) behaviour of poly(*N*-isopropylacrylamide) (pNIPAm) to induce a thermoresponsive attraction between nanoparticles.[16] While strategies for grafting pNIPAm polymers from the surfaces of nanoparticles have been described,[17] these involve rather complicated chemical protocols in the presence of the particles, such as surface-initiated free-radical or atom-transfer radical polymerizations. Here we take a more simple and versatile approach; we synthesize a surfactant based on pNIPAm. The addition of the chain-transfer agent, 1-octadecanethiol, to a free radical polymerization of pNIPAm results in C18-alkyl end-capped pNIPAm chains; thus a thermoresponsive surfactant is formed in a single step. This reaction can be performed on a large scale; in this study we prepare around 100 g of the surfactant with an estimated yield of approximately 92%. GPC analysis reveals a molecular weight $\overline{M}_n$ = 5.2 kg mol^{-1}, corresponding to approximately 45 NIPAm monomers per surfactant with a polydispersity $\overline{M}_w/\overline{M}_n$ = 2; this broad size distribution results from free radical polymerization and might in future work be improved through more controlled polymerization methods.[18]

2.1. Direct Measurement of Surface Forces

In CP-AFM (see **Figure 1**a), a large probe particle is glued to an AFM cantilever; bringing this colloidal probe in contact with a flat surface of identical chemistry allows the direct measurement of the force, *F*, between the surfaces as a function of their separation distance $h - h_0$.[19] After adsorbing the thermosensitive surfactant onto both the hydrophobic colloid and substrate, an attractive potential develops as the surfactant-coated system is heated above its LCST (Figure 1b), which we find to be 32 °C. Above the transition temperature an interface forms between the polymer-rich nanoscopic pNIPAm layer and the bulk solution; this interface is characterized by a low interfacial tension, calculated using JKR theory[20] to be approximately 10 mN m^{-1} at 35 °C, as measured using a surface force apparatus.[21] Upon contacting two opposing layers of this collapsed polymer, an adhesive interaction results between the two surfaces. Interestingly, this adhesive interaction continues to increase in strength as we increase the temperature above the LCST, from a total adhesion force of 0.2 nN at 32 °C to 3.4 nN at 44 °C. This suggests that the interfacial tension between collapsed pNIPAm and its surroundings are dependent on temperature (**Figure 2**a). We conclude that this is a direct consequence of the water content of collapsed pNIPAm above its LCST; this has been measured by various methods at 40 °C.[22] However, water content values appears to be very sensitive to the exact molecular weight and grafting density of the polymer.[21,23]

Additionally, we observe a clear dependence of the adhesion magnitude on the retraction velocity, v_r. We define the peak pull-off force, F_p, as the magnitude of the attractive minimum for each retraction curve; F_p clearly increases with an increase in v_r (Figure 2b). This is consistent with the separation of two polymeric brushes that have formed entanglements or other adhesive contacts.[24] This time-dependence on the adhesive forces obscures the true equilibrium interaction forces experienced by nanoparticles that are only thermally excited. To access the equilibrium adhesion, we extrapolate the peak pull-off force to $v_r = 0$. The interfacial or adhesion energy per unit area is estimated with the Dejaguin approximation using the exact size of our colloid probe ($2r$ = 8.6 μm), the extrapolated F_p ($v_r = 0$) and the interaction range, *L*. We estimate this interaction range by fitting the repulsive rise, at separations smaller than the attractive minimum, to a linear fit defining the constant compliance regime (solid line in Figure 2a) from which we approximate the true surface separation at F_p from the constant compliance line. We find that the $\langle L \rangle \approx 8$ nm for all investigated conditions

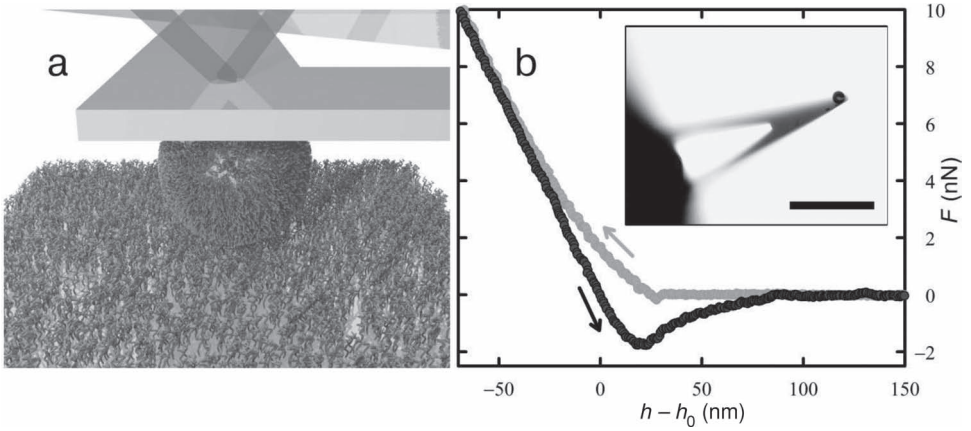

Figure 1. Colloid probe AFM: a) schematic of experimental set-up with absorbed thermoresponsive surfactant on the colloidal probe and flat substrate and b) typical raw approach (gray) and retraction (black) force–separation curves, for T = 38 °C, approach velocity, v_a' = 100 nm s^{-1}, and retraction velocity, v_r' = 100 nms^{-1}; inset: bright-field microscopy image of the colloidal probe on cantilever (scale bar 50 μm).

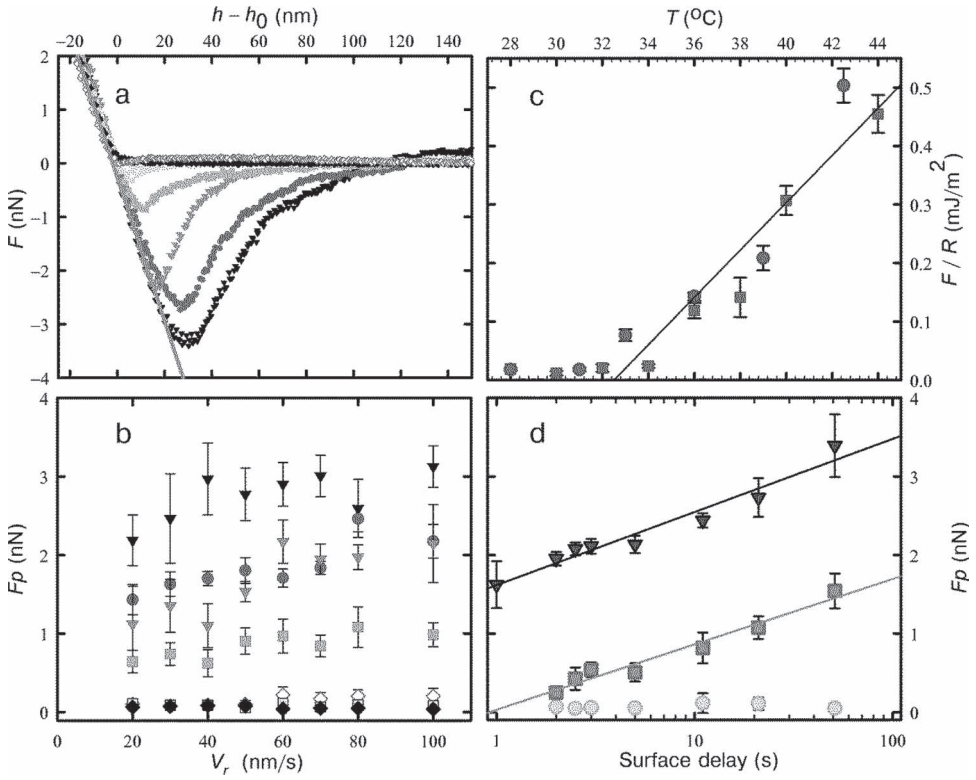

Figure 2. Force–separation curves at various temperatures in 0.05 g L^{-1} pNIPAm surfactant in 100 mM NaCl: a) retraction curves from bottom to top at $T = 44$, 40, 38, 36, 34, 32, and 28 °C with a constant contact time (10 s) and velocity ($v_r = 100$ nm s^{-1}); the solid line is a linear fit to determine the constant compliance regime for each retraction curve; b) averaged peak force, F_p, for at least 15 individual retraction curves at several velocities using large separation, $h - h_0$, values to normalize retraction curves; c) true adhesion energy using the Dejaguin approximation and the extrapolated F_p for $v_r = 0$; the line is a linear fit to temperatures above the LCST; and d) average peak force, F_p, versus contact time below (28 °C, ●) and above (36 °C, ■, and 45 °C, ▼) the LCST of the surfactant; the lines are logarithmic fits to the data.

as this length is predominately set by the R_g of absorbed surfactant; $R_g = bN^{0.5}$ where b is the Kuhn length, approximately 1.4 nm, and N the degree of polymerization for freely-jointed chains such as pNIPAm, measured to be approximately 45 (see the Supporting Information). This scaling results in an R_g = 9.4 nm which is in excellent agreement with <L>. The resulting interfacial energy shows a nearly linear dependence on temperature above the LCST (Figure 2c); this illustrates that within our simple approach the attractive force between nanoparticles is accurately tuned using temperature as a dial.

So far, we have shown results in which the contact time between the colloid probe and surface is held constant at 10 s. However, we may also vary the time that both surfaces are in contact by applying a surface delay between the approach and retraction curves; we aim to keep the surface in contact at a more-or-less constant load force of 10 nN. As we vary the contact time, we find a logarithmic increase in F_p with contact time for temperatures above the LCST (Figure 2d); this is reminiscent of aging of glassy contacts in other surface phenomena.[25] This aging of the adhesive contact, resulting in increasing peak force, is most likely a result of polymer chain interpenetration over time, which is a self-quenching process due to interpolymer friction.[24,26] Note that it could also be the result of hindered diffusion of water from the narrow collapsed polymer film between the two surfaces. The latter effect should saturate at long contact times which we do not observe and unfortunately longer surface delays become experimentally infeasible due to thermal drift of the cantilever. As a result, while the magnitude of the attraction between surfaces is tunable with temperature, the attraction is time-dependent. This feature, as we will show below, aids in the high-fidelity assembly of crystals and finally freezing in of the assembled structures over time.

2.2. Bulk Assembly

Nanoparticles onto which the pNIPAm-based surfactant is absorbed display temperature tunable self-assembly that is fully reversible. We adsorb the surfactant onto the surface by temperature cycling a suspension of particles above and below the LCST in the presence of the surfactant. In this manner, nearly any nanoparticle dispersion can be modified without complicated grafting methods.[17] Due to the equilibrium nature of surfactant adsorbtion some micelles are present in the bulk solution and in all experiments a small excess of surfactant is present; 50 mg L^{-1} is the concentration in solution. We use monodispersed sulfate-stabilized polystyrene nanoparticles synthesized through surfactant-free polymerization ($2r = 0.436$ μm). At temperatures below the LCST, the surfactant layer present on the particle surface acts to stabilize the dispersion, however upon heating to the LCST, the system undergoes reversible aggregation.

It should be emphasized that controlling the adhesion of individual nanoparticles onto the surface of the dispersion's container, such as coverslips or rheological geometries, is crucial. If the surface is unmodified, individual nanoparticles adsorb to the fixed boundary above the LCST preventing rearrangement and hindering efficient assembly. We prevent surfactant aborption at temperatures above the LCST to the container surface though the use of polyelectrolyte multilayers (PEMs).[27] For the rheological measurements, we do not modify the container walls to ensure stick boundary conditions.

The nanoparticle gels exhibit an elastic, solid-like response to an applied stress. We find that this elasticity originates from the stretching of individual attractive bonds between particles (see **Figure 3** and the Supporting Information), similar to the retraction process we performed in the AFM.[28] We montior the onset of elasticity in a concentrated suspension of pNIPAm-modified polystyrene particles upon heating the dispersion. This elastic response is measured using rheology by applying a small constant oscilliatory strain (γ = 0.2%) to the nanoparticle dispersion and calculating the in-phase storage (elastic, G') and out-of-phase loss (viscous, G') moduli.[29] As the dispersion is heated above the LCST of the surfactant, we find that the elastic modulus G' shows an immediate increase of several orders of magnitude followed by a slow approach to a plateau. Unlike other particle gel systems, G' and G'' are of the same order of magnitude, highlighting the highly flexible or dissipative interaction between individual nanoparticles (Figure S2 in the Supporting Information). The magnitude of this plateau increases linearly with the distance to the LCST, T–T_{LCST}. Remarkably, the magnitude of the elastic plateau of a bulk particle dispersion follows exactly the same linear dependence found in the colloidal probe AFM measurements (Figure 3c); this suggest a one-on-one relation between the forces measured with AFM and the macroscopic rheology. The elastic moduli of colloidal gels are typically governed by the stretching, not bending, of the interparticle bonds; $G' \approx \kappa(\xi)/\xi$, with $\kappa(\xi) \approx \kappa_0/N_{chain}$ where κ_0 is the individual bond spring constant, N_{chain} is the number of colloids in a stress bearing chain, and ξ is the mesh size of the network, which depends on the fractal dimension, d_f such that $\xi \propto 2r\phi^{-\frac{1}{3-d_f}}$ where φ is the volume fraction of colloids.[30,31] From these scaling arguments, we deduce that the magnitude of G' is dominated by the individual spring constant, κ_0, of the bond. In turn, the spring constant is taken to be the derivative of the force–extension curve of the bond, which is exactly what we measure in our AFM experiments.[32] Assuming there is little to no change in d_f and the measured interaction range is constant, <L> ≈ 8 nm, the resulting spring constant should be directly proportional to F_p. This is exactly what we see in our experiments from the excellent agreement between bulk rheology and individual force–extension curves.

Strikingly, the temperature-induced assembly, or aggregation, of these colloidal particles is fully reversible. We show the

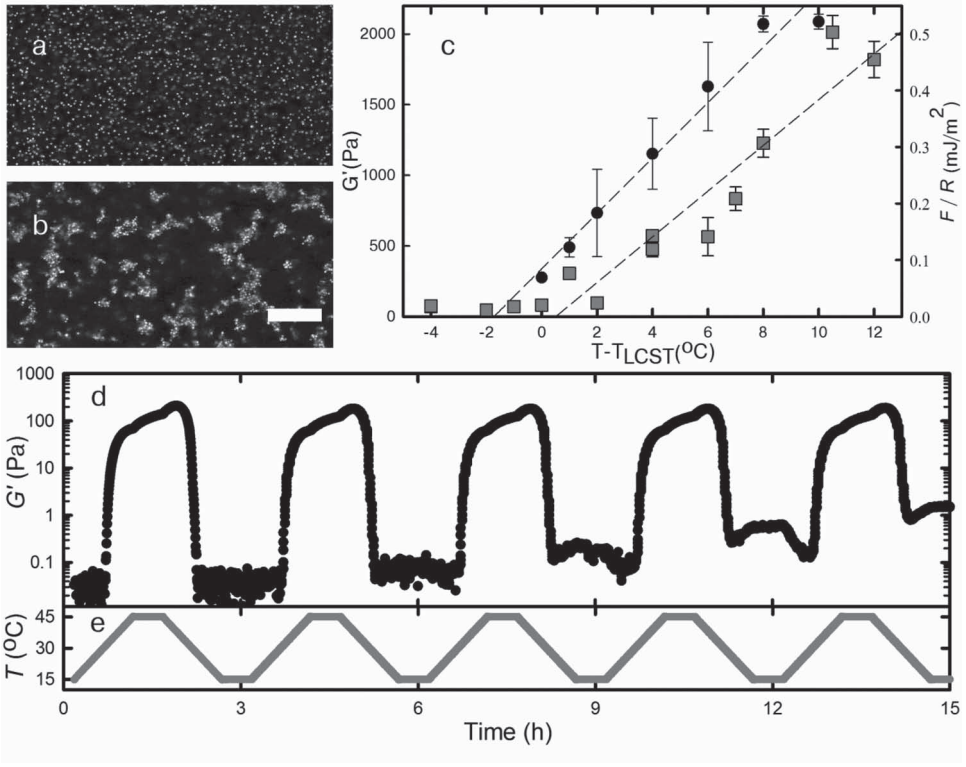

Figure 3. Temperature tunable bulk response of a nanoparticle dispersion, $2r$ = 436 nm with adsorbed surfactant in 0.05 g L^{-1} pNIPAm surfactant in 100 mM NaCl. Confocal reflectance microscopy of the nanoparticle dispersion a) below (T = 28 °C), and b) above (T = 40 °C) the LCST of the surfactant at volume fraction, φ, ≈5%, the scale bar represents 15 μm. c) Elastic modulus (G',•) as measured with oscillatory rheology of the particle dispersion at φ = 10% after 5 h at temperatures between 32 and 42 °C, and interfacial energy (■), measured by AFM, as in Figure 2c; the dashed lines are linear fits to the data. d) G' during 5 temperature cycles between 15 and 45 °C. e) temperature profile during cycling.

rheologic results of a temperature cycling experiment where a neutrally buoyant colloid dispersion is repeatedly heated and cooled between two temperatures above and below the LCST (Figure 3d and e). Heating and cooling rates are low, 0.5 °C min^{-1}, to minimize effects from convection. Additionally, the entirety of the measurement is performed in a oscillatory fashion with no preshear between cycles; we allow only diffusion to break up the elastic network. The network shows minor hysteresis as a background G' begins to rise after 5 cycles at temperatures below the LCST, although the magnitude of this background is still quite low, $G' \approx 1$ Pa.

2.3. Colloid-Scale Dynamics

At the individual colloid level above the LCST, the attractive potential causes not only the particles to assemble but also allows rapid rearrangement and crystallization. We follow this process using somewhat larger fluorescently labelled particles ($2r = 1.4$ μm; $\varphi \approx 5\%$) with a confocal microscope. We modify the surface of a two-dimensional chamber with a coating of a PEM, which eliminates adhesion of the nanoparticles to the walls of the sample chamber.

Upon heating a dispersion of nanoparticles confined in these chambers to above the LCST of the surfactant, isolated chains of small numbers of colloids ($N < 7$) form, which further assemble into larger crysallites (**Figure 4**a,b). The spatial configuration of these small assemblies is transient, suggesting highly "slippery" adhesive bonds. To illustrate this, we measure the bond angle, $\theta(t)$, between neighboring particles using standard particle-tracking algorithms.[33] Initially, the bond angles fluctuated rapidly, with the average angle $\langle\theta\rangle \approx \pi$ and the average number of bonds, $n_b \approx 2$, indicative of linear and "slippery" configurations. Over time, θ evolves until mechanically stable and energetically favorable equilateral triangle configurations, characteristic of hexagonal packings, form with $\theta \approx 1.05$ (60°) and $n_b = 3$ (Figure 4c; also see the movie in the Supporting Information). This process repeats until small hexagonal crystallite regions grow, limited only by the depletion of free particles and smaller assemblies in their surrounding area (Figure 4b). Interestingly, within these 2D crystallite regions colloids are still highly mobile; fluctuations in individual particle fluorescence intensity as each colloid moves in and out of the confocal volume occur throughout (Figure 4b; also see the movie in the Supporting Information). While individual bonds are clearly very attractive ($U >> kT$), the entire crystallite undulates due to thermal Brownian fluctuations. This combination of highly flexible yet persistent bonds formed between collapsed pNIPAm layers readily promotes the self-assembly of highly ordered structures. However, fluctuations in θ decrease with time above the LCST (Figure 4d,e), which may be due to an increase in bond strength with time, confirmed by the logarithmic increase in adhesion energy with contact time found in the AFM measurements (Figure 2d).

2.4. Triggered Emulsion Coalescence

Finally, we will illustrate that the same surfactant can be used to destabilize a suspension of droplets, thus triggering phase

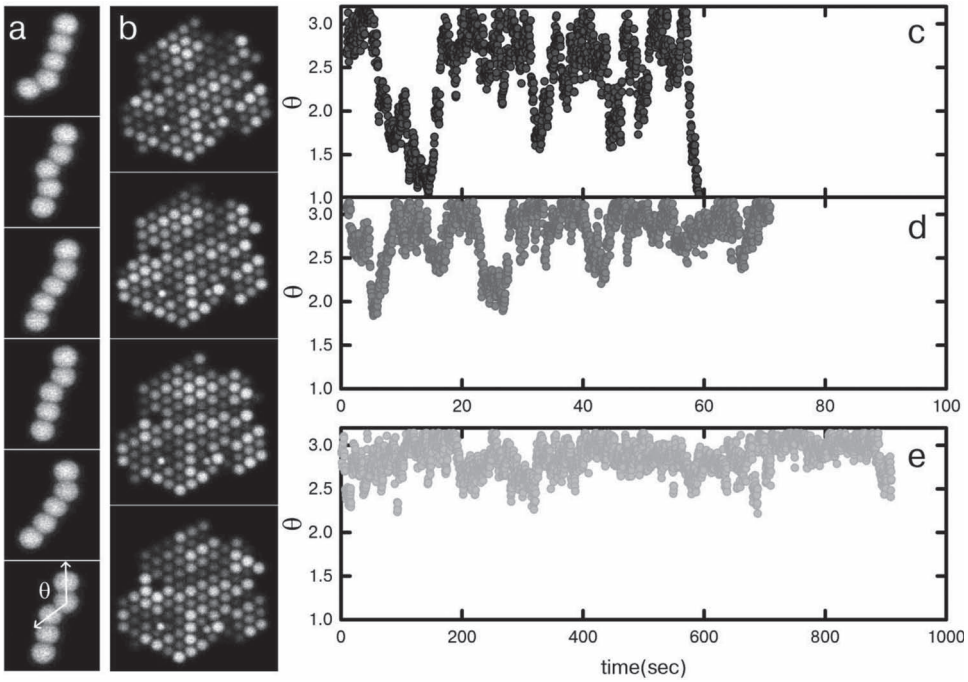

Figure 4. 2D confocal images of fluorescently labeled polystyrene colloids ($2r = 1.4$ μm, $\varphi \approx 5\%$) at 40 °C, above the LCST: a) time series of an isolated aggregated particle strand, $N = 5$; the time between images is 5 s; b) time series of a crystallite region; the time between images is 5 s; and c–e) neighboring bond angle, θ, for single chains with time for different incubation periods at 40 °C: 5, 20, and 60 min, respectively. θ is defined in the final frame of (a).

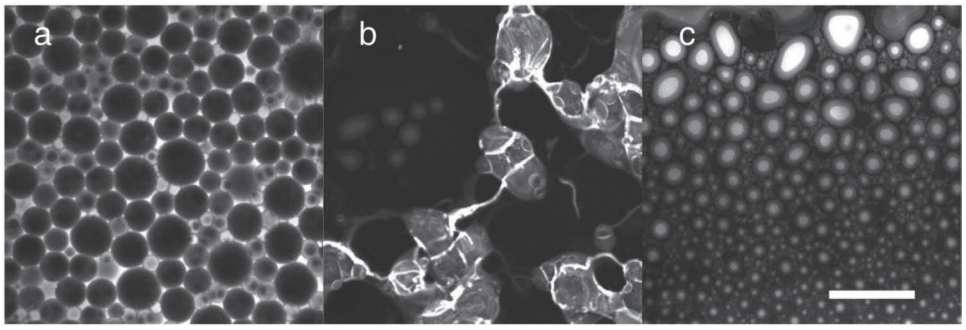

Figure 5. 2D slice using confocal microscopy of a decane emulsion ($\varphi \sim 65\%$) stabilized by the pNIPAm surfactant at: a) 22 °C, b) 45 °C, and c) after cooling back to 22 °C. The scale bar represents 50 μm.

inversion on demand. Phase inversion is relevant to many recovery and extraction processes,[15] while the actual mechanism of emulsion inversion is an area of active fundamental research;[34] enabling this process to occur on demand could enhance or prove a simple experiment method to investigate inversion. An emulsion stabilized by the thermoresponsive pNIPAm-based surfactant is very stable and concentrated gravitationally to a high droplet packing fraction without macroscopic or microscopic signs of droplet coalescence (**Figure 5**a). However, upon heating above the LCST of the surfactant, the droplets become adhesive and allows for rapid coalescence. Macroscopic phase separation ensues, leaving behind an aggregated network of collapsed surfactant (Figure 5b). Upon cooling, some of the emulsion spontaneously inverts (Figure 5c) permitting the oil to be recovered without chemical or mechanical breaking of individual droplets.

3. Conclusions

In this paper we have shown a new, and simple, method for inducing thermosensitive interactions to most hydrophobic nanoparticle suspensions. The adsorption of a thermoresponsive surfactant generates a temperature-tunable layer on the surface of the nanoparticle. Upon heating these particles above the LCST of the surfactant, the stabilizing polymer layer collapses and becomes adhesive. The magnitude of the adhesion energy, measured with colloid probe AFM, increases linearly with temperature and logarithmically with contact time. While such a logarithmic increase in interaction energy does prohibit rearrangement on longer timescales, the time necessary for small crystallites, of order 100 particles, to assemble is short, less than 10 min. The timescale for rearrangement is driven by Brownian motion and as our particles are relatively large ($2r = 1.4$ μm) compared to other assembly approaches,[26] we would expect smaller particles ($2r << 1.0$ μm) to assemble more efficiently. The logarithmic attraction with contact time could paradoxically serve to lock in the self-assembled structure, resisting mechanical vibration or fluid flow at long times. This simple, yet universal, approach presented here could lead to significant benefits in achieving high fidelity self-assembly of nanoparticle building blocks which so far has been difficult to control.

4. Experimental Section

Materials: All materials were purchased from Sigma-Aldrich and used as received, unless otherwise noted: 1-octadecanethiol, 2,2′-azobis(2-methylpropionitrile) (AIBN), ammonium persulfate (APS), carbon tetrachloride, chloroform, decane (99%), hexamethyldisilazane (HMDS), Nile red, *N*-isopropyl acrylamide (TCI America), poly(diallyldimethylammonium chloride) (PDADMAC) solution 20 wt% ($M_w \approx$ 400–500kDa), poly(sodium 4-styrenesulfonate) (PSS) solution 30 wt% ($M_w \approx$ 200 kDa), polystyrene ($M_w \approx$ 200 kDa), rhodamine B, sodium chloride (NaCl), sodium styrene sulfonate, styrene (99%), and tetrahydrofuran (THF, anhydrous, 99%).

pNIPAm Surfactant Synthesis: The PNIPAm-C18 surfactant was prepared by free-radical chain-tranfer polymerization. In a 500 mL round bottom flask, 1-octadecanethiol (3.4 g, 11.2 mmoles), NIPAm (100 g, 885 mmoles), and AIBN (3.8 g, 23.6 mmoles) are dissolved in THF (200 mL); the reaction molar ratios of thiol/NIPAm/AIBN were 1:75:2. The reaction was bubbled with argon for 15 min and heated to 55 °C overnight. The product was purified by precipitated into hexanes from THF, this was repeated twice and dried under vacuum. The molecular weight of the surfactant was characterized by gel permeation chromatography (GPC) with THF as the running solvent; $< M_w >$ = 5200, PDI = 2.0, degree of polymerization approximately 45 (see the Supporting Information).

Atomic Force Microscopy: Colloidal probe atomic force microscopy (CP-AFM) was used to directly measure the interaction forces between pNIPAm surfactant covered surfaces, as a function of temperature. All force measurements were carried out using a Nanoscope 3 AFM (Digital Instruments), equipped with a PicoForce scanner. Negatively charged sulfate modified polystyrene particles (Invitrogen, $2r = 8.6$ μm) as a colloidal probe were glued to a triangular, standard, contact-mode AFM cantilever (spring constant, $k = 0.1325 \pm 0.007$ N m^{-1}) using NOA61 (Norland Adhesives). It was confirmed that a single particle was attached to the cantilever before and after experiments with optical microscopy, as shown in the inset in Figure 1b. The bottom substrate for interaction measurements was prepared by spin-coating a thin layer of linear polystyrene dissolved in chloroform (1 wt%) onto a clean silicon wafer pretreated with HMDS using a Laurell WS-650-23 spin-coater.

After placing the modified substrate and AFM cantilever in a sealed liquid flow cell, a concentrated (5 g L^{-1}) surfactant solution was introduced to coat the surfaces with the thermoresponsive surfactant through adsorption. To ensure good coverage, the entire cell was heated to 45 °C, held for 15 min, the temperature was lowered to below the LCST and the system was flushed with the experimental solution in which all measurements were preformed, 0.05 g L^{-1} pNIPAm surfactant solution in 100 mM NaCl. Force–distance curves were measured using a scan range of 350 nm with scan rates ranging from 20 to 100 nm s^{-1} maintaining a contact time of 10 s between the probe and surface by varying the surface delay over a temperatures range from 27.0 to 40.0 °C. Additional force distance curves were collected at a fixed

approach and retraction velocity of 100 nm s^{-1} while varying the contact time from 1 to 50 s. At least 15 independent curves per temperature, scan rate, and contact time were recorded. The peak force was found by normalizing the large separation force of each curve to zero and locating the minimum.

Bulk Characterization: Several techniques were used to characterize the bulk dynamic processes as the stable colloidal dispersions were heated above the LCST of the adsorbed pNIPAm-C18 surfactant. Colloidal particles were synthesized using surfactant-free polymerization: in a sealed 1 L round-bottom flask equipped with an overhead paddle stirrer, deionized water (600 mL) and styrene (60 mL) were heated to 75 °C and bubbled with nitrogen for 15 min after which APS (0.6 g) predissolved in water (7 mL) was injected. The reaction proceeded for 36 h. The resulting polystyrene colloids ($2r$ = 0.436 µm, for distribution see the Supporting Information; SEM, Zeiss Supra 55) were washed into 1 wt% pNIPAm-C18 solution by centrifugation. To ensure good coverage, the temperature was raised to 40 °C during the final centrifugation cycle. The dispersion was washed into the experimental solution in which all our measurements were preformed: 0.05 g L^{-1} pNIPAm surfactant solution in 100 mM NaCl with 52 vol% D_2O to match the density of the dispersed phase to the polystyrene colloids. Oscillatory rheology was performed on an Anton Paar 501 rheometer using a double-walled couette geometry applying a strain of 0.2% at 1 Hz with a fixed heating rate of 0.5 °C min^{-1}. A preshear of g = 200 s^{-1} was performed between different temperatures (Figure 3c); no preshear was performed during temperature cycling (Figure 3d).

Colloidal Synthesis and 2D Microscopy: Fluorescence microscopy was used to visualize the flexibility of individual bonds between colloidal particles. Fluorescently labeled $2r$ = 1.4 µm polystyrene colloids were synthesized using dispersion polymerization.[35] The following were added to a 200 mL round-bottom flask: methanol (47.2 mL), water (8.4 mL), styrene (10.0 mL), AIBN (200 mg) and sodium styrene sulfonate (50 mg). The reaction was heated to 80 °C under reflux for 8 h. The suspension was filtered and washed by centrifugation (3×) into 1 wt% pNIPAm surfactant to a final $\varphi \approx$ 10%. To fluorescently label this dispersion, the particles were swollen with an aqueous miniemulsion of carbon tetrachloride ($\varphi \approx$ 10%), containing dissolved fluorophore (Nile red), stabilized by 1 wt% pNIPAm surfactant. The total carbon tetrachloride volume was 50 vol% to that of particle solids. This miniemulsion was added to the suspension of particles and stirred for at least 24 h. Nitrogen was blown over the solution at 50 °C for at least 6 h to evaporate the plasticizer (carbon tetrachloride). Free dye was removed from the colloidal dispersion by repeated centrifugation and redispersion in a 0.05 g L^{-1} pNIPAm surfactant solution with 100 mM NaCl.

2D microscopy imaging chambers were prepared with a polyelectrolyte multilayer (PEM) to ensure that colloids did not adhere to the chamber at temperatures above the LCST of the surfactant. Precleaned coverslides and coverslips were repeatedly immersed in 1 wt% pDADMAC in 2 M NaCl, rinsed with deionized water, 1 wt% pSS in 2 M NaCl, then rinsed, for a total of 6 polymer layers ending with an anionic PSS layer. A nearly 2D imaging volume was achieved by adding a very small volume of the colloidal dispersion (1 µL, $\varphi \approx$ 5%) to a PEM-treated coverslide, sealing the chamber with a PEM-treated coverslip and five-minute epoxy.

High-speed 2D imaging experiments were carried out on a low volume fraction suspension ($\varphi \approx$ 5% in 100 mM NaCl) using a Leica SP5 confocal microscope (100× oil objective) with a heated stage (Warner Instruments, WP-10) at 40 °C. Several thousands of images were captured at 50, 5, and 0.5 frames s^{-1} and precise particle locations found using standard centroid tracking algorithms. For Figure 4a,b, respectively, the pinhole was set to 3.0 airy units and then reduced to 0.5 airy units.

Confocal Microscopy: Confocal microscopy was used to visualize phase inversion of a oil-in-water emulsion stabilized by the pNIPAm-based surfactant. Experiments were carried out on a Zeiss Axiovert 200M microscope with objective and stage heaters (Warner Instruments, OW-1, WP-10). The emulsion was prepared at φ = 20% decane in 1 g L^{-1} surfactant solution, with a trace amount of rhodamine B, by homogenization. The emulsion was allowed to cream over several hours and a small volume at high volume fraction ($\varphi \approx$ 65%) imaged at 22 °C, heated to 40 °C, then cooled to 22 °C over approximately 30 min in total.

Supporting Information

Supporting Information is available from the Wiley Online Library or from the author.

Acknowledgements

J.S. acknowledges the Netherlands Organization for Scientific Research (NWO) for financial support. This work was supported by the Harvard MRSEC (DMR-0820484).The authors thank Dr. Maximilian Zieringer for performing the GPC measurements and Jeroen Appel for assistance during the experiments.

Received: June 6, 2012
Published online: September 10, 2012

[1] B. Hatton, L. Mishchenko, S. Davis, K. H. Sandhage, J. Aizenberg, *Proc. Natl. Acad. Sci. USA* **2010**, *107*, 10354.
[2] J. D. Forster, H. Noh, S. F. Liew, V. Saranathan, C. F. Schreck, L. Yang, J. G. Park, R. O. Prum, S. G. J. Mochrie, C. S. O'Hern, *Adv. Mater.* **2010**, *22*, 2939.
[3] D. S. Wiersma, P. Bartolini, A. Lagendijk, R. Righini, *Nature* **1997**, *390*, 671.
[4] X. Wu, H. Cao, *Opt. Lett.* **2007**, *32*, 3089.
[5] S. C. Glotzer, M. J. Solomon, *Nat. Mater.* **2007**, *6*, 557.
[6] J. D. Forster, J. G. Park, M. Mittal, H. Noh, C. F. Schreck, C. S. O'Hern, H. Cao, E. M. Furst, E. R. Dufresne, *ACS Nano* **2011**, *5*, 6695.
[7] D. Genovese, J. Sprakel, *Soft Matter* **2011**, *7*, 3889.
[8] M. P. Valignat, O. Theodoly, J. C. Crocker, W. B. Russel, P. M. Chaikin, *Proc. Natl. Acad. Sci. USA* **2005**, *102*, 4225.
[9] R. A. Sperling, W. J. Parak, *Philos. Trans. R. Soc. A* **2010**, *368*, 1333.
[10] C. Perruchot, M. Khan, A. Kamitsi, S. Armes, *Langmuir* **2001**, *17*, 4479.
[11] D. Chem, *Sol. Energy Mater. Sol. Cells* **2001**, *68*, 313.
[12] E. Dickinson, D. J. McClements, *Advances in Food Colloids*, Chapman and Hall, London **1996**, Ch. 5.
[13] R. Buscall, T. H. Choudhury, M. A. Faers, J. W. Goodwin, P. A. Luckham, S. J. Partridge, *Soft Matter* **2009**, *5*, 1345.
[14] Y. Liu, P. G. Jessop, M. Cunningham, C. A. Eckert, C. L. Liotta, *Science* **2006**, *313*, 958.
[15] C. H. Gao, *J. Petrol. Explor. Prod. Technol.* **2011**, *1*, 65.
[16] J. F. Lutz, O. Akdemir, A. Hoth, *J. Am. Chem. Soc.* **2008**, *128*, 13046.
[17] J. N. Kizhakkedathu, R. Norris-Jones, D. E. Brooks, *Macromolecules* **2004**, *37*, 734.
[18] W. Li, K. Min, K. Matyjaszewski, F. Stoffelback, B. Charleux, *Macromolecules* **2008**, *41*, 6387.
[19] W. A. Ducker, T. J. Senden, R. M. Pashley, *Nature* **1991**, *353*, 239.
[20] K. L. Johnson, K. Kendall, A. D. Roberts, *Proc. R. Soc. London A* **1971**, *324*, 301.
[21] I. B. Malham, L. Bureau, *Langmuir* **2010**, *26*, 4762.
[22] R. Pelton, *J. Colloid Interface Sci.* **2010**, *348*, 673.
[23] K. N. Plunkett, X. Zhu, J. S. Moore, D. E. Leckband, *Langmuir* **2006**, *22*, 4259.

[24] E. Spruijt, M. A. C. Stuart, J. van der Gucht, *Macromolecules* **2010**, *43*, 1543.
[25] O. Ben-David, S. M. Rubinstein, J. Fineberg, *Nature* **2010**, *463*, 76.
[26] P. L. Biancaniello, A. J. Kim, J. C. Crocker, *Biophys. J.* **2008**, *94*, 891.
[27] H. Zheng, I. Lee, M. F. Rubner, *Adv.Mat.* **2002**, *14*, 569.
[28] A. D. Dinsmore, V. Prasah, I. Wong, D. A. Weitz, *Phys. Rev. Lett.* **2006**, *96*, 185502.
[29] T. Gisler, R. C. Ball, D. A. Weitz, *Phys. Rev. Lett.* **1999**, *82*, 1064.
[30] W. H. Shih, W. Y. Shih, S. I. Kim, J. Liu, I. A. Aksay, *Phys. Rev. A* **1990**, *42*, 4772.
[31] Y. Kantor, I. Webman, *Phys. Rev. Lett.* **1984**, *52*, 1891.
[32] Y. Seo, W. Jhe, *Rep. Prog. Phys.* **2008**, *71*, 1.
[33] J. Crocker, D. G. Grier, *J. Colloid Interface Sci.* **1996**, *179*, 298.
[34] N. Bremond, H. Domejean, J. Bibette, *Phys. Rev. Lett.* **2011**, *106*, 241502.
[35] F. Zhang, L. Cao, W. Yang, *Macromol. Chem. Phys.* **2010**, *211*, 744.